On the Space–Time Scales of the Surface Solar Radiation Field

T. P. BARNETT, J. RITCHIE, J. FOAT, AND G. STOKES

Climate Research Division, Scripps Institution of Oceanography, La Jolla, California

(Manuscript received 9 September 1996, in final form 24 March 1997)

ABSTRACT

The characteristic space–time scales of surface solar radiation fields measured by the 111-instrument MESONET in Oklahoma are estimated after removal of the diurnal cycle. These estimates of ''within-day'' variability are used to deduce the representativeness of surface solar radiation measurements made at the central ARM measurement site as a function of time-averaging interval. Nomograms of the relation between point measurements and area averages are given for different space–time-averaging intervals. Examples from the nomograms show, for instance, that under conditions of low mean radiation (cloudy days), the central site point measurements are representative of a spatial area the size of a T42 GCM grid box (280 km × 280 km) if one uses hourly averages and is willing to accept a correlation of 0.45 between area average and point measurement. The point data represent a 60 km × 60 km region at a 0.90 correlation level if a 5-min time average is used. The characteristic timescale for the within-day radiation variability was roughly 60 min. Estimates of scale lengths for days when the mean background radiation conditions are high are also given in the nomographs.

1. Introduction

The principal goal of the Atmospheric Radiation Measurement Program (ARM) is to obtain data that will be useful in improving the parameterization of clouds in general circulation models or GCMs (Stokes and Schwartz 1994). With this goal in mind, an extensive field program has been initiated in Oklahoma to obtain the necessary measurements. The field site consists of a central location where an enormous set of cloud and radiation data are being collected. Coming on line is also an array of other, much more limited measurement sites intended to set the central site observations in perspective.

A major question arises in trying to relate the central site ARM data to today's GCMs: the data are taken at a single point location but the GCMs address average conditions in a grid box that is typically several hundred kilometers on a side. How does one relate the point measurements to the large area average? The main purpose of this article is to indicate a simple way in which this might be accomplished for surface solar radiation data.

The problem noted above is not much different from the satellite instrument verification problem wherein one tries to verify remotely sensed data representative of a spatial ''footprint'' against individual measurements within the footprint. This aspect of the verification problem has been addressed by Pierson (1983) and Brown et al. (1982) who used trade-offs between time averaging and space averaging, underpinned by the Taylor hypothesis, to compare satellite estimates of surface wind with various forms of direct wind measurements.

In the meteorology community, the most recent work to relate point measurements to area averages is that of Long and Ackerman (1995) who tried to interrelate atmospheric measurements from an array of pyranometers during the First ISSCP Radiation Experiment. In this work, the diurnal cycle dominates most of the results. Its removal decreased spatial correlation as one would expect. They conclude that one can space measurement sites roughly 150 km apart if one is interested in using daily averaged radiation data. In the current paper, we inquire about the statistical properties of the subdaily timescales, that is, the nature of the variability about the diurnal cycle.

Subsequent sections of this paper describe how data from the Oklahoma MESONET were used to determine a way of relating single location data to information representative of a much larger area. The MESONET data were used instead of the comparable data from the ARM array since the former array has been operational long enough to provide the required data that is only now beginning to flow from the latter array. Plus, the MESONET is a far denser array than the ARM array. We consider first a general description of the MESONET and its measurements. The properties of the MESONET, as an array, are investigated next and then approaches are discussed for converting point measurements at the central ARM site to areally representative constructs.

Corresponding author address: Dr. T. P. Barnett, Climate Research Division, Scripps Institution of Oceanography, University of California, San Diego, La Jolla, CA 92093-0224.
E-mail: tbarnett@ucsd.edu

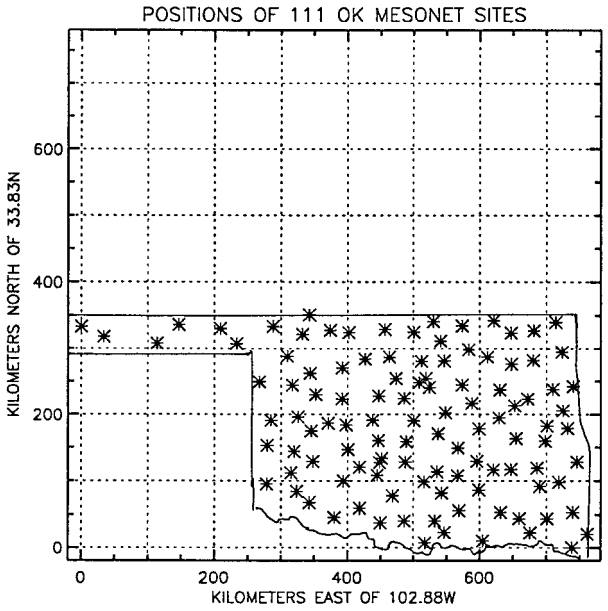

FIG. 1. The ''*'s'' indicate the locations of the 111 MESONET measurement sites.

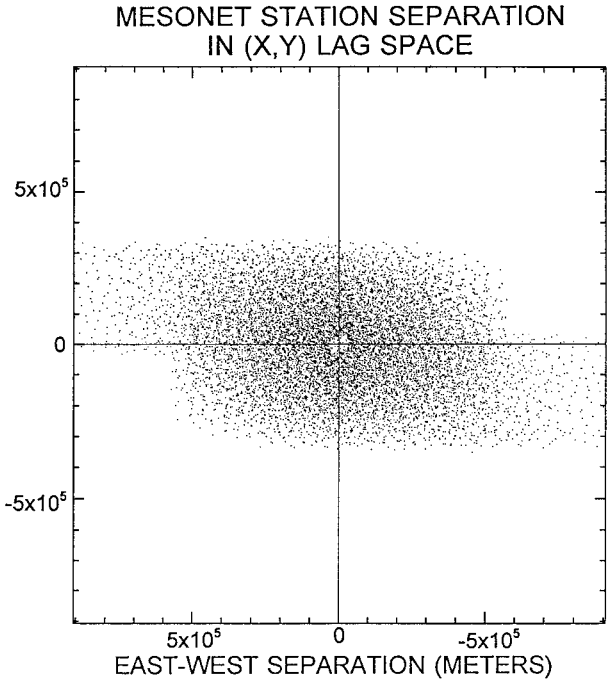

FIG. 2. MESONET station separation in two-dimensional lag space.

2. The MESONET

The data used in this study were obtained from instruments deployed as part of the Oklahoma MESONET (Brock et al. 1995). The MESONET consists of 111 stations deployed throughout the state of Oklahoma, with at least one station in each county (Fig. 1).

The solar radiation data used in this study was collected using a silicon photo diode detector (a Licor 200). The detector is located at a 1.75-m height on a platform positioned south of the meteorologic tower associated with each station. The calibration of the instrument is based on a comparison with an Eppley Precision Spectral Pyranometer. Brock et al. (1995) note that the claimed absolute accuracy of such a calibration is 5%. The instrument dome is cleaned regularly but not daily. Both the temperature and radiation sensors are sampled at 3-s intervals and then averaged into 5-min mean values.

The MESONET radiation data used in this study were for the months of June, July, and August 1994. Each month was analyzed separately as described in the later sections. Prior to analysis, each time series was visually inspected. Obviously bad data and/or data gaps were omitted in the calculations noted below. Some days had enough missing or problematical data that they were excluded from the analysis altogether. Suffice it to say, potential users of this raw dataset ought to be cautious, as it is rough.

3. Array characteristics of the MESONET

Consider the MESONET as an array for the measurement of variables that have their own frequency–wavenumber spectrum, $E(l, m, \omega)$, where (l, m) are the (x, y) components of wavenumber $k^2 = l^2 + m^2$ and ω the circular frequency. A properly designed array will be omnidirectional and homogeneous with respect to the scales of interest. This means that information, for example, a plane wave incident upon the array, will not have its characteristic length–time scale distorted or otherwise dependent upon the direction from which it approaches the array. In such a situation, the array provides an unbiased estimate of the spectrum of whatever signal it is observing. It seems worth describing the array characteristics of the MESONET since this apparently has not been previously done.

The physical position of MESONET measurement sites in Oklahoma were shown in Fig. 1. But the important information for the current analysis is the distribution of products of station data in lag space. Define the time series of data from the station located at position (x_i, y_i) to be $u_i(t)$. The two-dimensional spatial correlation function is

$$C(X, Y) = [u_i(x_i, y_i, t)u_j(x_j, y_j, t)]_t, \qquad (1)$$

where $X = x_i - x_j$ and $Y = y_i - y_j$ while the time average is only taken for ''good'' data. With 111 MESONET stations, there are 6105 different pairs of separation or lag (X, Y) values and the distribution of these are shown in lag space in Fig. 2. It is immediately clear that the lag space is not only well sampled, but the distribution of pairs is relatively homogeneous in the space. The ''wings'' extending to the left and right in the space are due physically to stations in the ''panhandle'' of the state.

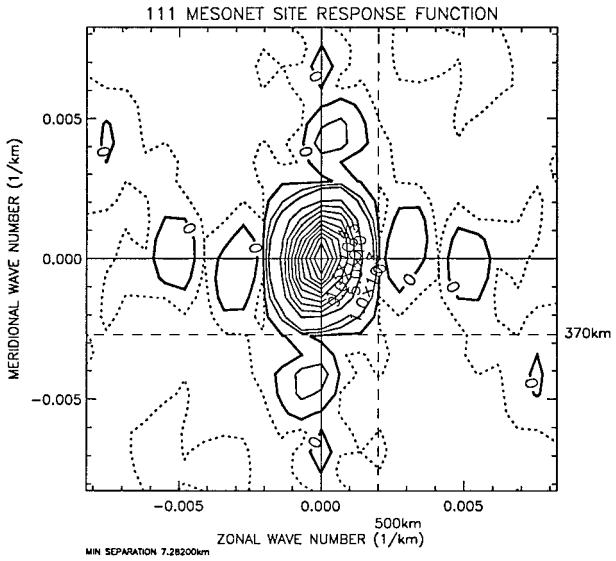

FIG. 3. MESONET array response function. The array should resolve well waves with east–west scales and north–south scales up to 500 and 370 km, respectively.

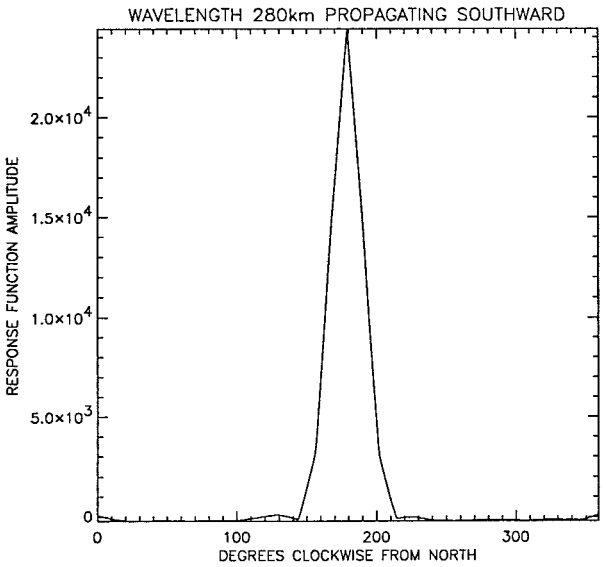

FIG. 4. MESONET array response for a wavelength of 280 km propagating from north to south over the array.

Measurement at discrete locations means the true estimate of C will appear as if it had been multiplied by a factor $g(X, Y)$ that is zero everywhere except at locations (X, Y) in lag space where there is a simultaneous observation pair. At those locations, g has unit value, but everywhere else it is zero. Thus, the estimated spectrum is

$$\hat{E}(l, m) = \int \int_{-\infty}^{\infty} E(l_o, m_o)G(l - l_o, m - m_o)\, dl_o\, dm_o. \tag{2}$$

It may be shown (e.g., Barber 1963) that the response function of the array can be defined as

$$G(l, m) = \int_{-\infty}^{\infty} \int g(X, Y) \exp - i2\pi(lX + mY)\, dX\, dY. \tag{3}$$

If G has a wide spread in (l, m) space, the array has poor resolving power and will distort or blur incident wave information. Ideally, G is sharply peaked for length scales that one wishes to study.

The function given in (3) was evaluated via numerical integration for a wide range of possible incident Fourier components and the resulting array response shown as function of wavenumber (l, m), compare Fig. 3. The zero crossings of the response function are at 500 km for zonally (l) traveling waves and 370 km for meridional (m) waves. Variations with length scales less than these values are well resolved by the MESONET down to distances of order 30 km. Thus, scales smaller than those associated with, say, a T42 GCM whose grid interval is roughly 280 km are well sampled spatially by the MESONET. However, waves simulated by such a GCM will be at least two grid intervals (560 km) and so not well resolved by the MESONET. By way of example, Fig. 4 shows the response function amplitude for a wave with 280-km wavelength propagating southward. The directional resolution is to within plus/minus 15° (half power points on the response function), but, more important, there are virtually no sidelobes to alias the signal.

In summary, the distribution of measurement stations in the Oklahoma MESONET is nearly ideal for relating subgrid-scale processes to scales associated with a typical, state-of-the-art GCM grid box. However, the array is not well suited to studying the longer waves produced by a GCM

4. Data processing

A fast major task was to remove the diurnal signal from the radiation data. This apparently simple preprocessing was required, else the daily signal would dominate the analysis. It turned out that the most effective way to do this was to consider a typical or average day for a given month, and then use this average day as a basis for normalizing the data for the entire month.

More precisely, consider the radiation field $u_i(t) \equiv u(i, d, t)$, where i = station number (maximum value N), d = day of the month (maximum value D), and t = time of day. We first truncated u, eliminating the first and last two hours of daylight data, for example, early morning and early evening, to filter these poorly defined values. We then defined the typical or average day for the month by averaging u over i and d:

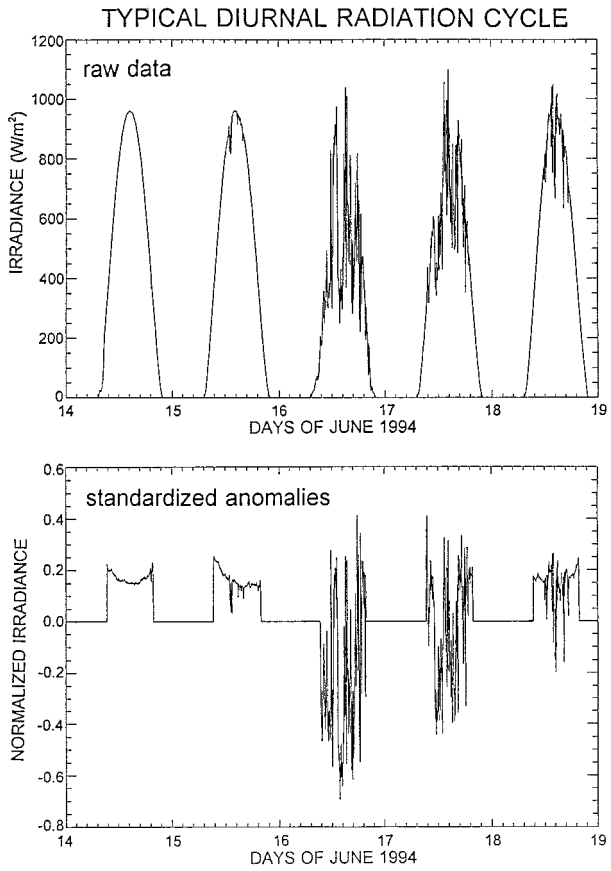

FIG. 5. Typical irradiance data for five June days: (a) raw data and (b) standardized irradiance according to (5).

$$s(t) = \frac{\sum_{i,d}^{N,D} u(i, d, t)}{ND}. \quad (4)$$

We take $s(t)$ to be representative of the daily cycle for a particular month. To formally remove the daily signal from the data, we define the normalized time-dependent radiation field at position i by

$$n(i, d, t) \equiv \frac{u(i, d, t) - s(t)}{s(t)}. \quad (5)$$

The normalized dataset allows for a meaningful comparison of the radiation field not only between different days and stations, but also between different times of day. Typical daily time series of incident radiation before and after removal of the daily cycle and normalization are shown in Fig. 5. A number of features of the data are apparent. As can be deduced from the sunny days in the figure, the above approach was not entirely successful in removing the daily signal. This is because a daily signal independent of both geographical location in the state and time of month was used in the normalization. However, from the figure we can also see that the daily signal residual is dwarfed by that due to cloud activity. This is not true for sunny days when the ''within-day'' variability is small. The normalized dataset has the advantage that it accentuates any variability in the data due to cloud attenuation and minimizes that due to the daily cycle. The small traces of the diurnal cycle that remain were removed from each day's data by fitting and subtracting a simple second-order polynomial function of time. Note the difference in latitudes of the stations, the ''cosine^2 problem,'' does not effect the following calculations since the means are removed as just noted and we look only at temporal variability.

In order to simplify and order the analysis, we found it desirable to divide the data up into two categories: ''sunny'' days, characterized by high daily mean incident radiation, and ''cloudy'' days, characterized by low daily mean incident radiation. Clearly, there is subjectivity in such characterizations, but we have tried to make the distinction quantitative by using two different methods.

1) The total daily radiation received at a station was computed from the raw data. The one-third highest values at a selected station were termed sunny days, while the one-third lowest values were termed cloudy.
2) Utilizing the advantages of the normalized dataset, we computed the average and standard deviation of $n(i, d, t)$ over i and t. We found that this provided a natural way to distinguish between sunny and cloudy days. A sunny day should have a high average and a low standard deviation, indicating that there was a reasonably steady, but large, amount of radiation measured. A cloudy day should have a low average and a (perhaps) high standard of deviation, thus indicating that the radiation was highly variable throughout the day. Bilinear analysis of these two variables showed two fairly distinctive groups from which we could identify cloudy and sunny days.

It is clear that other definitions of these two situations could be used and might give somewhat different groupings. We performed the analyses described below using both definitions. Fortunately, the results were not highly sensitive to the definitions.

A final problem with the data has potentially serious consequences. It often happened that a day would have an extended period that was sunny and extended periods wherein the radiation fluctuated more dramatically, that is, it was cloudy. The daily time series then represents a nonstationary process that is difficult to analyze by traditional methods (but see section 7). The worst of these daily time series were excluded from subsequent analysis by both numerical and visual filtering since their analysis presents statistical problems well beyond the scope of the present introductory study. This resulted in a loss of about one-third of the original data. As noted by a reviewer, this could conceivably introduce bias into our results and conclusions. Unfortunately, it is not clear which way the bias might operate.

In summary, our data processing has left us with information on the within day variability of the surface radiation field, variability that remained after removal of the diurnal cycle, conditional on the daily mean radiation being high or low. The data is representative of spatial scales that are generally subgrid scale by GCM standards.

5. Estimating a representative scale: A simple approach

We selected a station in the middle of the MESONET (Spencer, OK) as a ''central'' site. Denote radiation measurements at that station by $d(x_0, T/t)$, with spatial location given by x_0. The data is in time series format but has been averaged in time over successive intervals T and so differs from the raw data u or standardized data n. All of the other observed time series in the MESONET array were also individually time averaged over successive intervals T and were represented by $d(x, T/t)$. Next, we computed the spatial average of the $d(x, T/t)$ that lie within a preselected radial distance, R, of x_0. This average, $\overline{d}(R, T/t)$, does include $(x_0, T/t)$. Denote, the simple correlation between the two time series, $d(x_0, T/t)$ and $\overline{d}(R, T/t)$, by $r(R, T)$. This analysis compares an area average with a point measurement and so is relevant to the problem of relating ARM CART observations to a GCM grid box. The metric $r(R, T)$ can also be thought of as representative of the spectrum of mesoscale within-day radiation variability expressed in physical space.

We repeated the identical analysis for the four stations immediately surrounding Spencer and then averaged the five estimates of r together to get a statistically stable estimate of the relation between point and area average measurements as functions of time. It is important to remember that we are investigating the within-day variability due to mesoscale processes and not the average properties of the daily total radiation field.

A contour map of the average is shown in the ''two space'' defined by the *radial averaging* distance R and the *temporal averaging* time T (Fig. 6). As expected, the values of r are large for small R and increasing T. In the limit of R approaching 0, then r will be identically equal to one for all T. In this case, this occurs at $R =$ 30 km, the minimum bin size–station spacing that includes only the station at x_0. Likewise, for large R and small T, we expect r to be small (as observed).

When one selects a spatial scale comparable to a T42 GCM grid box, that is, a radial distance of about 140 km, one needs to use averaging times of order 2 h, in order to have a correlation of 0.60 between the central site and the average of the radiation field within a ''T42 GCM grid box'' for sunny day formulations. For cloudy days, the central site is representative of a grid box less than 70 km on a side at $r = 0.60$. Even longer averaging times will produce higher correlations for both cloudy and sunny days. Thus, the expected correlation between

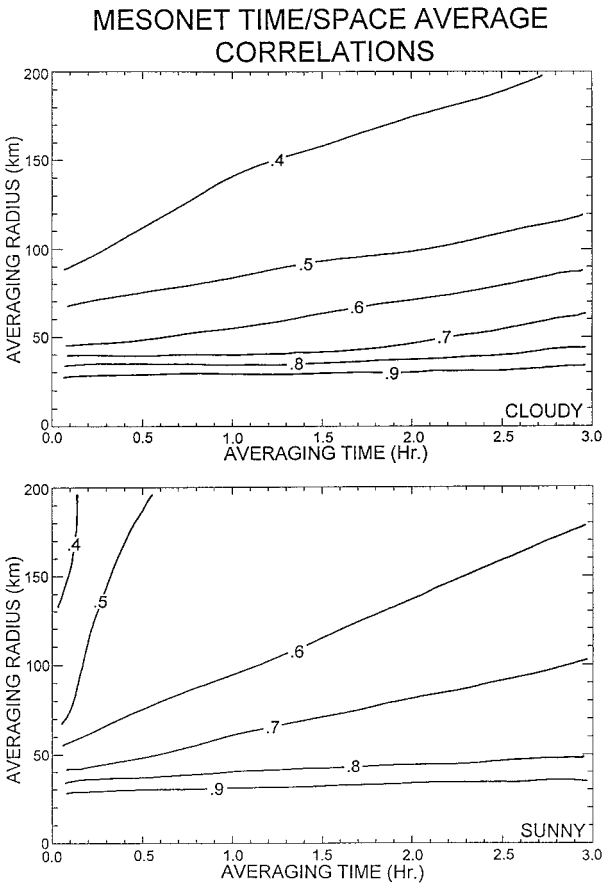

FIG. 6. Correlation between a single site at the center of the MESONET array and the average of the station data around the site as functions of radius of the averaging area and interval of time averaging for cloudy conditions (top) and clear-sky conditions (bottom).

the central site measurements and average conditions over, say, a T42 box around the central site is under 0.6 (the correlation value at $R = 140$, $T = 120$ min), so they share only about 36% common variance. Investigators have to select a correlation value they are comfortable with and that selection will determine the time average, call it T', that must be applied to the central site data to make the latter ''representative'' of the GCM-scale radiation field.

The results shown in Fig. 6 lead to several interesting situations. For instance, if one selects a correlation level of, say, 0.60 and intends on testing a T42 model, then T' is approximately 120 min (sunny days) and even more for cloudy days. But the integration time step for a typical T42 model is of order 20 min. This means that the central site data cannot be used to test the fundamental timescale of a T42 radiation code, but only the output of such code if it is averaged over five to six time steps. Given the current state of radiation modeling, this does not seem like much of a constraint.

Another interesting situation is that for the longest

averaging time that was statistically feasible,[1] 3 h, the maximum correlation is of order 0.90 for cloudy days and minimum station separation (30 km). This means that the central site is only capturing 80% of the variance represented by the area average of a very high resolution grid, say T216. A correlation of 0.9 between the central site and a grid box comparable to a T42 grid cannot be realized. In both cases, any model validation made from the central site data alone will be less than optimal. Use of a daily average will increase the correlation value, as found by Long and Ackerman (1995), but apparently not be so useful for considerations of within-day variability.

6. The classical approach

It is well known in classical sampling theory that the characteristic timescale for a process is the time lag at which the autocorrelation of the process has its first zero crossing, that is, its decorrelation time (e.g., Bendat and Piersol 1971). This is the effective time required to achieve another independent sample of the process. In analogy, the characteristic scale length of a process is associated with the first zero crossing of its spatial correlation function (1). Thus, the spatial representativeness of the central site can be obtained from this function, as estimated from the MESONET array data, provided the array is sampling a homogeneous process. The zonal/meridional length scales (Lx, Ly), where the correlation function goes to zero, gives another measure of the areal region that is being sampled by the central site. Put another way, this means that measurements at the central site will likely not be representative of conditions more than a distance of (Lx, Ly) away from it. These characteristic scales, estimated below for different time-averaging intervals, T, can be compared directly with those discussed in section 5.

The two-dimensional spatial correlation functions for the radiation field were computed for cloudy/sunny days from data that had been averaged in time over different intervals; much the same strategy used in section 5. A typical smoothed example of such a calculation averaged over June, July, and August is shown in Fig. 7. In constructing this figure, we found the zero crossing contour was poorly defined, even after extensive smoothing. The 0.1 contour on the other hand, was well defined and stable. Thus, we took it as a conservative estimate of the length scales of the MESONET radiation field. The location of this pseudozero crossing increases with averaging time as one would expect, although the changes were small for timescales beyond about 60 min. Surprisingly, the scales for which the values are statistically different from zero, the shaded regions, for time averages of 5, 60, and 180 min on cloudy days, are all roughly equivalent and equal to about 75 km (see below). On sunny days, the pseudozero crossing scale increases with averaging time, but again the change between 60 min and 3 h is not large. Again, the significant region increases only marginally with increasing averaging time. The correlation functions for either sky condition are marginally isotropic, a result more or less independent of the averaging time. This is especially true if one concentrates just on the values that differ significantly from zero. This result implies the isotropic averaging process used in section 5 was appropriate.

In any event, the characteristic scale length for either sky condition is about 300 km if one considers only the pseudozero crossing criteria and 3-h averaging periods. This estimate of the scale length is strongly dependent on the low frequency content of the data; for example, even a small residue of the diurnal cycle will greatly exaggerate the estimate of scale length. All things considered, this estimate, while traditional, may not be the best one to use given the unique nature of the radiation data.

The dependence of correlation function die away on averaging time suggests another way to define the representativeness of the central site. The correlation estimates, such as shown in Fig. 7, have uncertainty associated with them, so there is associated uncertainty in defining the zero crossing. Knowing this uncertainty, one can define the zero crossing as the point where the correlation becomes statistically indistinguishable from zero, that is, where its 95% confidence limits first includes zero. We estimated the number of temporally independent pairs of values that were used to compute the two-dimensional spatial correlation functions and, assuming each day's measurements were independent, the confidence limits on those functions. The 0.05 interval is shown as the shaded regions of the illustrations. Considering a scale length defined by correlation values that are statistically significant from zero yields a value of about 75 km. The length scales are much smaller as noted above but still nearly independent of averaging time. This results from the fact that for longer averaging times, there are fewer degrees of freedom and so the confidence limits increase. In this case, the larger confidence limits and the effect of time averaging balance to leave the significant spatial scale length essentially unchanged. In any event, the typical scale lengths obtained by this approach are in reasonable agreement with those found in section 5.

7. Temporal considerations

So far we have only discussed the characteristic spatial scales of the radiation field. It is also important to know the characteristic timescale of the field, that is, the decorrelation time of the radiation time series. In the process of estimating the temporal degrees of freedom for the significance tests mentioned in section 6, we found that

[1] In the sense that enough realizations were available to do the statistical analyses used in this study.

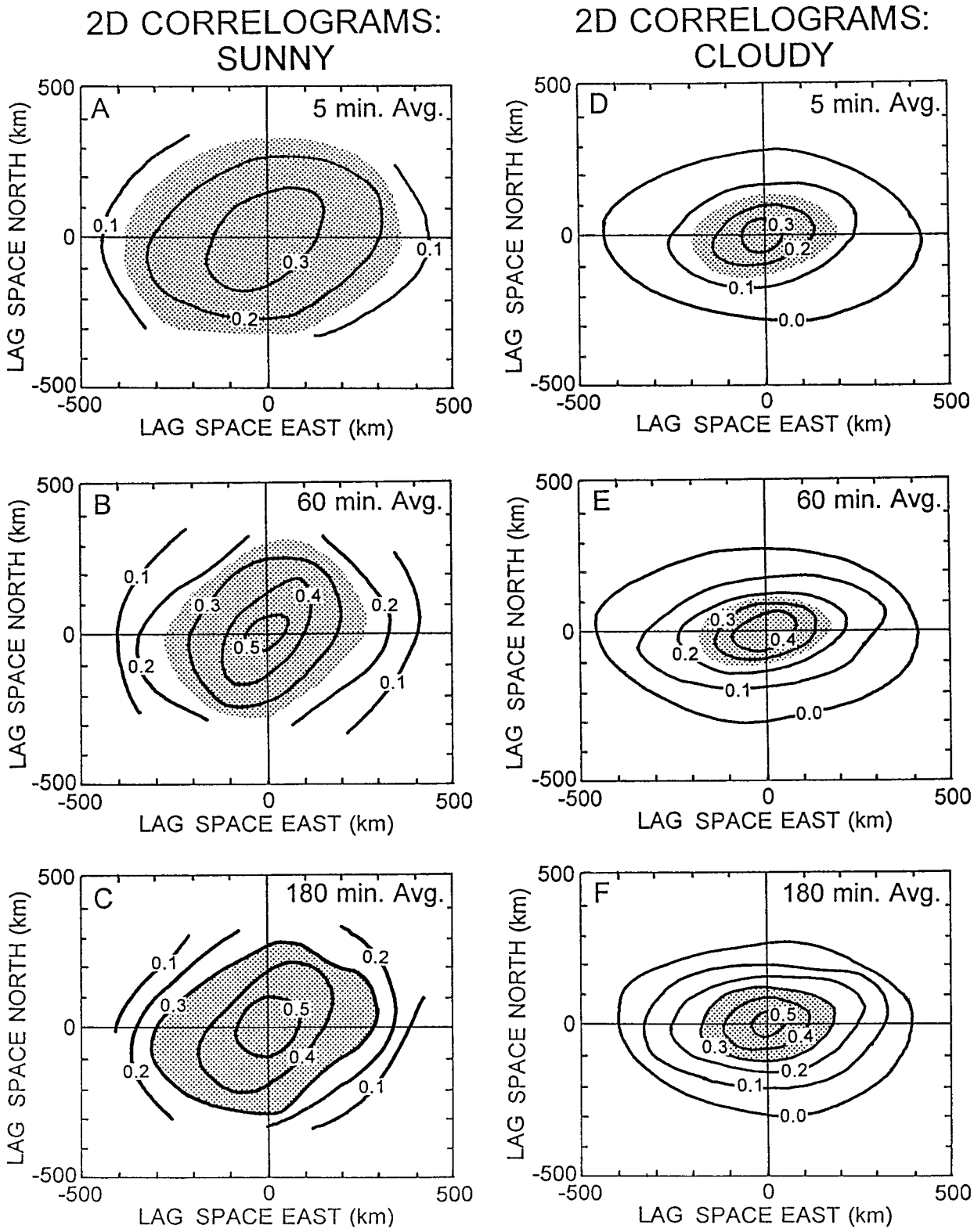

FIG. 7. Two-dimensional correlation function for (a) sunny and (b) cloudy days for data-averaging times of 5, 60, and 180 min. The shaded regions are 0.05 confidence levels.

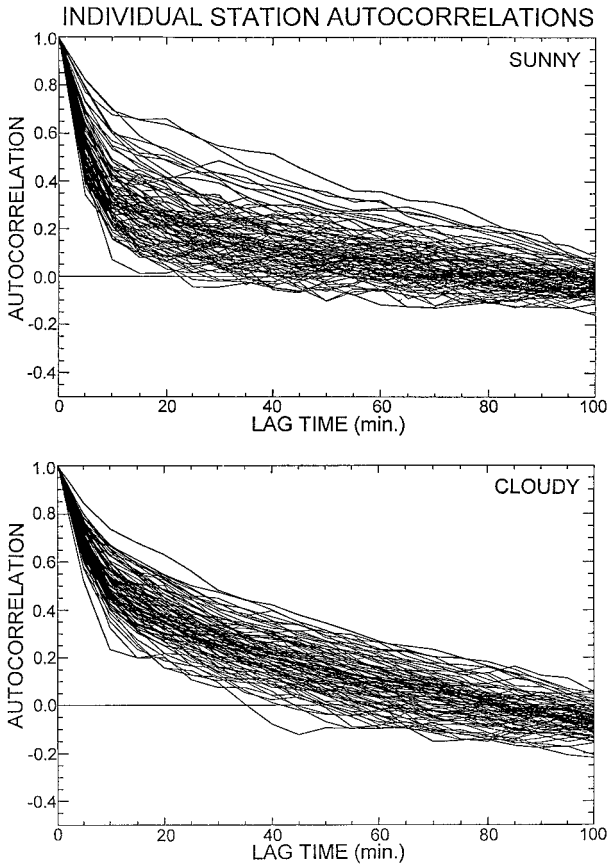

FIG. 8. Typical swarm of daily station autocorrelation functions for sunny (top) and cloudy (bottom) days.

the temporal autocorrelation function, computed from 5-min data of individual radiation time series, typically first had zero crossings at about 60 min for either sunny or cloudy conditions. According to Fig. 6, this averaging time corresponds to a spatial radial scale for cloudy conditions of approximately 40 km if one selects an r of 0.80 or 140 km (T42 scale) if one settles for an r about 0.4. Thus, averaging times beyond the roughly 60-min interval produce new realizations of the radiation field at individual stations, but do so slowly due to the length of the characteristic timescale. Averaging these new realizations would reduce noise and cause $C(X, Y)$ to die away more slowly. This effect will not be so noticeable in the estimates of section 5 since the weighting of the simple correlation by the more numerous near-field pairs will tend to dominate the result.

The decorrelation time of about 60 min noted above was typical of all the stations in the MESONET during cloudy conditions for all three summer months studied. This characteristic time tended to be only a little shorter during sunny conditions, although the correlation function decayed more quickly in such conditions. There was considerable variability in the day-to-day estimates as shown in Fig. 8. In any event, the similarity of the results suggests that the spectrum of mesoscale processes affecting the within-day radiation field must be near saturation (or a similarity form) most of the time, although there is clearly some dependence on mean background state.

Given the tendency for the radiation time series to be nonhomogenous, we also estimated the timescale through the structure function (Tatarskii 1961). This estimate is a cousin to the correlation function and is defined for a simple time series $n(t)$ by

$$D(\delta) = \{[(n(t) - n(t + \delta)]^2\}.$$

The structure function works well for piecewise stationary time series and can be shown to produce results identical to the correlation function for stationary time series. In this case, the timescale is given by the time lag at which D becomes constant, independent of δ. During sunny conditions, the structure function produced values of the characteristic timescale that were approximately 40 mins averaged over all stations and all summer months. Under cloudy conditions, the timescale was closer to 120 mins. The disparity in the cloudy day timescales suggests the nonstationarity noted above may be affecting the correlation estimate and so the result of the structure function analysis may be more reliable.

Practically, the results of this section imply that the central site data is limited in its ability to describe within-day spatial variations in the radiation field. As shown in Fig. 6, this limitation is dependent on the level of sameness one desires between the single site and the area average it is claimed to represent. If one accepts the characteristic timescale of about 1 hr for sunny days, the central site can represent an area average comparable to a T42 grid cell only if one accepts a site-area average correlation of order 0.55, that is, 30% of the area average—point measurement variance in common. On cloudy days, if we accept a 2-hr timescale from the structure function analysis, then Fig. 6 suggests an area average—point measurement correlation of just over 0.40 (16% shared variance).

There is a final critical question that we cannot answer in the present work: What mesoscale physical processes are responsible for the time (and space) scales found in our analysis? Could they involve mesoscale cloud clusters? Or perhaps the horizontally extensive, but very thin vertically, lens of enhanced water vapor found in the lower troposphere over the Oklahoma site (Melfi et al. 1995; Cooper et al. 1996). It is hoped that in a follow-up study we will be able to offer an explanation for our numerical results. But at this point we do not have the ancillary data to make such suggestions.

8. Summary

Several approaches have been taken to estimate how well the ARM central site surface solar radiation data, observations taken at a single location, represent different size area averages. This is a critical estimate to

know if one is going to use the central site data to validate grid-scale GCM radiation estimates.

The shortwave radiation data from the dense Oklahoma MESONET array was used to determine the relation between point measurements and area averages. Prior to analysis, the diurnal cycle was removed from the data so we are studying variations in radiation about the diurnal cycle or what we termed within-day variability. It turns out that the degree of similarity between the point measurements and area averages depends on averaging time of the data and the state of the cloud field. Further, investigators must decide on the degree of similarity (correlation) they are willing to accept between a point value and area average. For instance, on cloudy days, if one requires a correlation of 0.9 between point measurements and associated area averages, then the central site will represent a region with radius 30 km, for example, a grid cell appropriate to a spectral resolution of about T216. If one relaxes the level of agreement to a correlation of 0.45, about 20% shared variance, the GCM grid box size increases to about 250 km or T42 resolution.

If the MESONET data for the period of study are representative, they suggest a decorrelation time in the within-day shortwave radiation field of roughly 60 mins for sunny days and perhaps twice that long for cloudy days. This, in turn, implies a limit on the spatial area that a single-point measurement can represent. The limit is again conditional on the level of similarity between the point measurement and area average that one is willing to accept.

The physical processes that gave rise to the scale lengths estimated here are currently unknown. However, the within-day variability in the radiation field between sunny and cloudy days was not as large as one might expect. This in turn implies that the mesoscale physics responsible for the variability may not be radically different between the two mean radiation states. Unfortunately, there were not adequate data available in the current study to even develop reasonable hypothesis. However, with the ARM extended array now operational and the close tie-in with numerous satellite data sources, this shortcoming can hopefully be remedied in the near future.

Acknowledgments. Support for this work was provided by DOE Grant DE-FG03-91-ER61198. We wish to thank Debbie Gracio, Robin Perez, and the ARM Experiment Center Staff for their prompt and attentive provision of data and responses to our requests and inquiries. We would also like to acknowledge our EST representative Rick Cederwall and Peter Lamb, Martin J. Leach, and Michael E. Splitt for their support. Special thanks are due to Nick Graham for useful discussions on this work. We also appreciate the useful suggestions provided by reviewers.

REFERENCES

Barber, N. F., 1963: The directional resolving power of an array of wave detectors. *Ocean Wave Spectra,* Prentice Hall, 137–150.

Bendat, J. S., and A. G. Piersol, 1971: *Random Data: Analysis and Measurement Procedures.* Wiley-Interscience, 407 pp.

Brock, F. V., K. C. Crawford, R. L. Elliott, G. W. Cuperus, S. J. Sadler, H. L. Johnson, and M. D. Eilts, 1995: The Oklahoma MESONET: A technical overview. *J. Atmos. Oceanic Technol.,* **12,** 5–19.

Brown, R. A., and Coauthors, 1982: Surface wind analyses for SEASAT. *J. Geophys. Res.,* **87** (C5), 3355–3364.

Cooper, D. I., W. E. Eichinger, S. Barr, W. Cottingame, M. V. Hynes, C. F. Keller, C. F. Lebeda, and D. A. Poling, 1996: High-resolution properties of the equatorial Pacific marine atmospheric boundary layer from lidar and radiosonde observations. *J. Atmos. Sci.,* **53,** 2054–2075.

Long, C. N., and T. P. Ackerman, 1995: Surface measurements of solar irradiance: A study of the spatial correlation between simultaneous measurements at separated sites. *J. Appl. Meteor.* **34,** 1039–1046.

Melfi, S. H., D. Whiteman, R. Ferrar, and K. Evans, 1995: Study of the atmospheric water vapor using a Raman lidar. *Rev. Laser Eng.,* **23,** 108–111.

Pierson, W. J., Jr., 1983: The measurement of the synoptic scale wind over the ocean. *J. Geophys. Res.,* **88** (C3), 1683–1708.

Stokes, G. M., and S. E. Schwartz, 1994: The Atmospheric Radiation-Measurement (ARM) Program: Programmatic background design of the cloud and radiation test bed. *Bull. Amer. Meteor. Soc.,* **75,** 1201–1221.

Tatarskii, V. I., 1961: *Wave Propagation in a Turbulent Medium.* McGraw-Hill, 285 pp.